Effects of ambient pressure, gas temperature and combustion reaction on droplet evaporation

Tomoaki Kitano, Jun Nishio, Ryoichi Kurose*, Satoru Komori

Department of Mechanical Engineering and Science, and Advanced Research Institute of Fluid Science and Engineering, Kyoto University, Kyoto daigaku-Katsura, Nishikyo-ku, Kyoto 615–8540, Japan

Abstract

The effects of ambient pressure, initial gas temperature and combustion reaction on the evaporation of a single fuel droplet and multiple fuel droplets are investigated by means of three-dimensional numerical simulation. The ambient pressure, initial gas temperature and droplets' mass loading ratio, ML, are varied in the ranges of 0.1-2.0 MPa, 1000-2000 K and 0.027-0.36, respectively, under the condition with or without combustion reaction. The results show that both for the conditions with and without combustion reaction, droplet lifetime increases with increasing the ambient pressure at low initial gas temperature of 1000 K, but decreases at high initial gas temperatures of 1500 K and 2000 K, although the droplet lifetime becomes shorter due to combustion reaction. The increase of ML and the inhomogeneity of droplet distribution due to turbulence generally make the droplet lifetime longer, since the high droplets' mass loading ratio at local locations causes the decrease of gas temperature and the increase of the evaporated fuel mass

*Corresponding author. Tel.:+81 75 383 3610; fax: +81 75 383 3613.
Email address: kurose@mech.kyoto-u.ac.jp (Ryoichi Kurose)

fraction towards the vapor surface mass fraction.

Key words: Droplet evaporation, Spray combustion, High pressure, Numerical simulation

1. Introduction

Spray combustion is utilized in many industrial devises such as gas turbine engine, diesel engine and so on. Recently, the spray combustion behavior has been studied by means of two- or three-dimensional direct numerical simulation (DNS) (e.g., [1–17]) or large-eddy simulation (LES) (e.g., [18–22]). However, the mechanism of spray combustion has not been fully understood yet. In particular, the effects of ambient pressure on the spray combustion behavior have not been well clarified yet mainly because the combustion conditions and the acquired properties are extremely limited due to the difficulty of the measurements (e.g., [23–25]).

Droplet evaporation is one of the most important factors which strongly depends on ambient pressure and therefore changes the spray combustion behavior in high ambient pressure conditions. Miller et al. [26] examined the validity of evaporation models by comparing them with experimental results in detail. Also, Miller and Bellan [27] performed a three-dimensional DNS and discussed the effects of the initial liquid mass loading ratio, initial Stokes number, and initial droplet temperature on the droplet evaporation in a turbulent mixing layer. In these studies, however the ambient pressure was fixed at the atmospheric pressure of 0.1 MPa and therefore the effects of the ambient pressure on the droplet evaporation were not studied.

The effects of the ambient pressure on the droplet evaporation have been

investigated for a single droplet or an array of droplets. Nomura and Ujiie [28] experimentally studied the evaporation rate of a single droplet at various ambient pressures in the range of 0.1-5.0 MPa, and showed the pressure dependence of droplet lifetime. Yang and Wong [29] performed a numerical simulation of a flow around a single evaporating droplet under the same conditions as the Nomura and Ujiie's experiments. They suggested that the heat conduction from a fiber used in the experiment to suspend the droplet and the radiation from the furnace wall strongly affect the droplet evaporation rate. Similarly, Harstad and Bellan [30] numerically investigated the evaporation rate of a single droplet at various ambient pressures in the range of 0.1-10.0 MPa, and validated the evaporation models in sub- and supercritical conditions. They stated that precise estimation of Lewis number is essential in supercritical conditions. On the other hand, Mikami et al. [31] studied the burning lifetime of interacting two droplets at various ambient pressures in the range of 0.1-6.0 MPa by experiments, and showed that the pressure dependence of the burning lifetime for the interacting droplets is similar to that of a single droplet. That is, the total interaction coefficient, which is the ratio of the burning lifetime of the interacting droplets to that of a single droplet, slightly changes. In these studies, however, the evaporation characteristics of multiple droplets have not been discussed.

The purpose of this study is therefore to investigate the effects of ambient pressure, initial gas temperature and combustion reaction on the evaporation characteristics of both a single fuel droplet and multiple fuel droplets by means of three-dimensional numerical simulation. The ambient pressure, initial gas temperature and mass loading ratio are varied in the ranges of

0.1-2.0 MPa, 1000-2000 K and 0.027-0.36, respectively.

2. Numerical Simulation

2.1. Governing equations

Present numerical simulation is performed based on the Euler-Lagrange framework. The governing equations for the gas phase are the conservation equations of mass, momentum, energy and mass of each species as

$$\frac{\partial \rho}{\partial t} + \nabla \cdot (\rho \boldsymbol{u}) = S_\rho, \tag{1}$$

$$\frac{\partial \rho \boldsymbol{u}}{\partial t} + \nabla \cdot (\rho \boldsymbol{u}\boldsymbol{u}) = -\nabla P + \nabla \cdot \boldsymbol{\sigma} + S_{\rho u}, \tag{2}$$

$$\frac{\partial \rho h}{\partial t} + \nabla \cdot (\rho h \boldsymbol{u}) = \frac{\partial P}{\partial t} + \boldsymbol{u} \cdot \nabla P + \nabla \cdot (\rho a \nabla h) + S_{\rho h}, \tag{3}$$

$$\frac{\partial \rho Y_k}{\partial t} + \nabla \cdot (\rho Y_k \boldsymbol{u}) = \nabla \cdot (\rho D_k \nabla Y_k) + S_{comb,k} + S_{\rho Y_k}, \tag{4}$$

and the equation of state for ideal gas [2, 5–7]. Here ρ is the density, $\boldsymbol{u}$ the gas phase velocity, P the pressure, $\boldsymbol{\sigma}$ the viscous stress tensor, h the specific enthalpy, and a the gaseous thermal diffusivity given by $\rho a = \lambda / c_p$, respectively. Here λ is the heat conductivity. Y_k and D_k are the mass fraction and the mass diffusion coefficient of the k-th species which is given under the unity Lewis number assumption as $\rho D_k = \lambda / c_p$, respectively.

The phase coupling between the gas and dispersed-droplets phases is calculated by a Particle-Source-In-Cell (PSI-Cell) method [32], and the source terms, S_ρ, $S_{\rho u}$, $S_{\rho h}$, and $S_{\rho Y_k}$, are given as

$$S_\rho = -\frac{1}{\Delta V} \sum_N \frac{dm_d}{dt}, \tag{5}$$

$$S_{\rho u} = -\frac{1}{\Delta V}\sum_{N}\frac{dm_d \boldsymbol{u}_d}{dt}, \tag{6}$$

$$S_{\rho h} = -\frac{1}{\Delta V}\sum_{N}\frac{dm_d h_d}{dt}, \tag{7}$$

$$S_{\rho Y_k} = -\frac{1}{\Delta V}\sum_{N}\frac{dm_d}{dt} \quad \text{for} \quad Y_k = Y_F, \tag{8}$$

where ΔV is the volume of the control volume for the gas phase calculation, m_d the droplets' mass, $\boldsymbol{u}_d$ the droplet velocity, h_d the specific enthalpy of a fuel droplet, and N the number of fuel droplets in the control volume. $S_{comb,k}$ is the source term due to the combustion reaction, as described later.

Concerning the evaporation of fuel droplets, a non-equilibrium Langmuir-Knudsen evaporation model [26, 27, 33] is employed. The governing equations for each droplet's position, $\boldsymbol{x}_d$, velocity, $\boldsymbol{u}_d$, temperature, T_d, and mass, m_d, are given by

$$\frac{d\boldsymbol{x}_d}{dt} = \boldsymbol{u}_d, \tag{9}$$

$$\frac{d\boldsymbol{u}_d}{dt} = \frac{f_1}{\tau_d}(\boldsymbol{u} - \boldsymbol{u}_d), \tag{10}$$

$$\frac{dT_d}{dt} = \frac{Nu}{3Pr}\left(\frac{c_p}{c_{p,d}}\right)\left(\frac{f_2}{\tau_d}\right)(T - T_d) + \frac{1}{m_d}\left(\frac{dm_d}{dt}\right)\frac{L_V}{c_{p,d}}, \tag{11}$$

$$\frac{dm_d}{dt} = \dot{m}_d. \tag{12}$$

Here T is the gas temperature, c_p the specific heat of mixture gas, $c_{p,d}$ the specific heat of the droplet, L_V the latent heat of evaporation at T_d, and τ_d the particle response time defined by

$$\tau_d = \frac{\rho_d d_d^2}{18\mu}, \tag{13}$$

where ρ_d is the droplet density, μ the viscosity and d_d the droplet diameter. The Prandtl and Nusselt numbers in the gas phase are given by

$$Pr = \frac{\mu}{\rho a}, \quad Nu = 2 + 0.552 Re_{sl}^{1/2} Pr^{1/3}. \tag{14}$$

The droplet Reynolds number based on the slip velocity, $U_{sl} = |\boldsymbol{u} - \boldsymbol{u}_d|$, is defined as

$$Re_{sl} = \frac{\rho U_{sl} d_d}{\mu}. \tag{15}$$

The corrections of the Stokes drag and heat transfer for an evaporating fuel droplet, f_1 and f_2, are given as [2, 26, 34].

2.2. Evaporation model

Recently, various evaporation models have been proposed and validated [26, 27, 33, 35–39]. In this study, a non-equilibrium Langmuir-Knudsen evaporation model is used [26, 27, 33]. The effect of the temperature gradient inside the droplet is neglected here due to its small effect [26]. As the liquid fuel, n-heptane and n-decane are used. Evaporation rate in Eq.(12) is given as

$$\dot{m}_d = -\frac{m_d}{\tau_d} \left(\frac{Sh}{3Sc} \right) \ln(1 + B_M), \tag{16}$$

[26, 27, 33], where Sc and Sh are the Schmidt and Sherwood numbers given as

$$Sc = \frac{\mu}{\rho D_k}, \quad Sh = 2 + 0.552 Re_{sl}^{1/2} Sc^{1/3}, \tag{17}$$

and B_M is the mass transfer number given by

$$B_M = \frac{Y_{F,s} - Y_F}{1 - Y_{F,s}}. \tag{18}$$

Here Y_F is the mass fraction of fuel vapor in the far-field condition for a fuel droplet which is represented by the value in the cell where the fuel droplet is

located (this condition is the same for $\boldsymbol{u}$ and T), and $Y_{F,s}$ is the vapor surface mass fraction (i.e., saturated vapor mass fraction) given as

$$Y_{F,s} = \frac{X_{F,s}}{X_{F,s} + (1 - X_{F,s})\overline{W}/W_F}, \tag{19}$$

$$X_{F,s} = \frac{P_{sat}}{P} - \left(\frac{2L_k}{d_d}\right)\beta, \tag{20}$$

where $X_{F,s}$ is the mole fraction of fuel vapor at the droplet surface, P_{sat} the saturated vapor pressure discussed later, P the pressure of the carrier gas, and $\overline{W}$ and W_F the averaged molecular weight of the carrier gas and the molecular weight of the fuel vapor, respectively. In Eq.(20), the non-equilibrium effect is considered using the Langmuir-Knudsen evaporation law, in which the non-dimensional evaporation parameter, β, is given by

$$\beta = -\left(\frac{\rho_d Pr}{8\mu}\right)\frac{dd_d^2}{dt}. \tag{21}$$

The value of the Knudsen layer thickness, L_k, is estimated by

$$L_k = \frac{\mu\left\{2\pi T_d(R/W_F)\right\}^{1/2}}{ScP}. \tag{22}$$

Here R is the universal gas constant.

2.3. Saturated vapor pressure

In many cases, the saturated vapor pressure, P_{sat}, in Eq.(20) is calculated by

$$P_{sat} = P\exp\left\{\frac{L_V W_F}{R}\left(\frac{1}{T_B} - \frac{1}{T_d}\right)\right\}. \tag{23}$$

This equation is derived from the Clausius-Clapeyron equation;

$$\frac{dP_{sat}}{dT} = \frac{L_V W_F}{T(v_g - v_l)}, \tag{24}$$

under the assumptions of constant L_V and ideal gas, where v_g and v_l are the molar volumes of the gas and liquid phases, respectively. However, the validity of these assumptions have not been fully examined. Here T_B is the boiling temperature which can be calculated from Sato's expression for non-polar substance [40] as

$$T_B = \left(\frac{P^{0.119} - C_1}{11.9} \right)^{1/0.119}, \tag{25}$$

where C_1 is the experimental constant. For n-decane and n-heptane, C_1=−22.4066 and C_1=−21.9011 are used, respectively. It should be noted that, the unit of P is [mmHg] in this expression.

In order to exactly solve Eq.(24), it should be numerically integrated using the exact L_V, v_g and v_l. The variable L_V is estimated by using the Watson equation [41] as

$$L_V = L_{V,B,atm} \left(\frac{T_c - T_d}{T_c - T_{B,atm}} \right)^{0.38}, \tag{26}$$

where $T_{B,atm}$ is the normal boiling temperature, T_c the critical temperature, and $L_{V,B,atm}$ the latent heat at $T_{B,atm}$. On the other hand, v_g and v_l are calculated using the equation of state for real gas and the equation of corresponding states correlation, respectively. As these equations, Peng-Robinson equation [42] and Gunn-Yamada equation [43] are used, respectively. The Peng-Robinson equation is described as

$$v_g = \frac{RT}{P} z, \tag{27}$$

where z is the compressibility factor given by

$$z^3 - (1 - C_3)z^2 + (C_2 - 3{C_3}^2 - 2C_3)z - (C_2C_3 - C_3^2 - C_3^3) = 0, \tag{28}$$

$$C_2 = \frac{aP}{R^2T^2}, \quad C_3 = \frac{bP}{RT},$$

where a and b are calculated as

$$a = 0.45724\frac{R^2T_c^2}{P_c}\alpha, \tag{29}$$

$$\alpha^{1/2} = 1 + (0.37464 + 1.54226\omega - 0.26992\omega^2)(1 - T_r^{1/2}),$$

$$b = 0.07780\frac{RT_c}{P_c}. \tag{30}$$

Here P_c is the critical pressure and $T_r = T/T_c$ the reduced temperature. The values of acentric factor, ω, for n-decane and n-heptane are 0.488 and 0.349, respectively [44]. The Gunn-Yamada equation is described as

$$v_l = v_r^{(0)}(1 - \omega\Gamma)v_{sc}, \tag{31}$$

$$v_{sc} = \frac{RT_c}{P_c}(0.2920 - 0.0967\omega),$$

where $v_r^{(0)}$ and Γ are calculated with T_r as

$$v_r^{(0)} = \begin{cases} 0.33593 - 0.33953T_r + 1.51941T_r^2 - 2.02512T_r^3 + 1.11422T_r^4 \\ \qquad\qquad (0.2 \leq T_r \leq 0.8) \\ 1.0 + 1.3(1 - T_r)^{1/2}\log_{10}(1 - T_r) - 0.50879(1 - T_r) \\ \qquad -0.91534(1 - T_r)^2 \quad (0.8 < T_r < 1.0), \end{cases} \tag{32}$$

$$\Gamma = 0.29607 - 0.09045T_r - 0.04842T_r^2 \quad (0.2 \leq T_r < 1.0). \tag{33}$$

On the other hand, empirical expressions for P_{sat} have been proposed by Antoine [45] and Sato [40] based on the measurements. The Antoine's expression [45] is described as

$$\log_{10} P_{sat} = C_4 - \frac{C_5}{T + C_6}, \tag{34}$$

where C_4, C_5 and C_6 are the experimental constants. For n-decane, C_4=4.07857, C_5=1501.268 and C_6=−78.67 are used, and for n-heptane, C_4=4.02832, C_5=1268.636 and C_6=−56.199 are used. It should be noted that, the unit of P_{sat} is [bar] in this expression. The Sato's expression for non-polar substance [40] is descried using Eq.(25) as

$$P_{sat}^{0.119} = 11.9T^{0.119} + C_1. \tag{35}$$

It should be noted that, the unit of P_{sat} is [mmHg] in this expression.

Fig.1 shows the comparison of saturated vapor pressure, P_{sat}, against droplet surface temperature, T_d, calculated by Eqs.(23), (24), (34) and (35) for n-decane and n-heptane. As the integration method of Eq.(24), the 3rd oder Runge-Kutta method is used. While the exact prediction of P_{sat} by Eq.(24) are in good agreement with the empirical expressions by the Antonie [45] and Sato [40], the assumed prediction by Eq.(23) overestimates them. Accordingly, the Sato's expression [40] is employed in the present computations.

2.4. Computational details

Fig.2 shows the schematic of the computational domain and initial droplet distributions. The computational domain is a cube 5 mm on a side and is divided into 50 uniform computational grid points in each direction. This number of grid points was determined by comparing the computational results obtained by computations with 50^3 and 100^3 grid points. The differences in droplet lifetime described later between them were less than 1.3 % for all cases. The computations are performed for the evaporation of a single fuel droplet and for the evaporation/combustion reaction of multiple

fuel droplets. Initially, the single fuel droplet and multiple fuel droplets are allocated at the center of the computational domain and in the central region as a spherical shape with 2 mm diameter, respectively. The initial droplet diameters are set to 700 μm for a single fuel droplet and 7.5 μm for multiple fuel droplets. These droplet sizes are decided to compare with the experiments [28] and to meet the requirement associate with the grid size from the point of view of numerical accuracy, respectively (the grid spacing needs to be roughly 10 times larger than the droplet size to get enough accuracy by using the PSI-Cell method [10]). The initial droplet temperature is 300 K. As the fuel, n-decane and n-heptane are used for the evaporation of a single fuel droplet, whereas n-decane is used for the evaporation/combustion reaction of multiple fuel droplets.

The combustion reaction of the evaporated n-decane ($C_{10}H_{22}$) with oxygen is described using a one-step global reaction model [46] as

$$C_{10}H_{22} + \frac{31}{2}O_2 \longrightarrow 10CO_2 + 11H_2O, \tag{36}$$

and the reaction rate is given by the Arrhenius formulation as

$$\frac{\rho}{W_F}\dot{\omega} = AT^n \exp\left(\frac{-E}{RT}\right)\left(\frac{\rho Y_F}{W_F}\right)^a \left(\frac{\rho Y_O}{W_O}\right)^b. \tag{37}$$

Here $\dot{\omega}$ is the combustion rate of the fuel, W_F and W_O are the molecular weights of the fuel and oxidizer, respectively. A is the frequency factor, T the gas temperature, E the activation energy, and a, b and n the parameters depending on the fuel. In Eq.(4), the source term of the k-th species, $S_{comb,k}$, is expressed using the combustion rate of the fuel, $\dot{\omega}$, as

$$S_{comb,k} = -\frac{n_k}{n_F}\frac{W_k}{W_F}\rho\dot{\omega}, \tag{38}$$

where n_k and n_F are the molar stoichiometric coefficients of the k-th species and the fuel in the one-step global reaction (positive for the productions), respectively. W_k and W_F are the molecular weights of the k-th species and the fuel, respectively.

Table 1 lists the numerical conditions performed for the evaporation / combustion reaction of the multiple fuel droplets in this study. The ambient pressure, P, initial gas temperature, T_0, and droplets' mass loading ratio, ML, are varied in the ranges of 0.1-2.0 MPa, 1000-2000 K, and 0.027-0.36, respectively. Here ML is the ratio of the total mass of fuel droplets to the mass of gas in the spherical region. In order to investigate the effects of combustion reaction and inhomogeneity of droplet distribution, the computations are carried out for different mediums of the ambient gas (i.e., nitrogen and air) and the initial droplet distributions (i.e., random and inhomogeneous). Here the inhomogeneous droplet distribution is obtained by the DNS data for the droplet distributions in a isotropic turbulence in Matsuda et al. [47]. In order to increase ML of inhomogeneous droplet distributions, a parcel model [2] in which one parcel represents two fuel droplets is applied. These cases with the parcel model are indicated using superscription * as 4^*, 11^*, 17^* and 19^* in Table 1. In the table, G is the Group combustion number [48] given as

$$G = \frac{3}{4} Le (2 + 0.552 Re_{sl}^{1/2} Sc^{1/3}) n_T^{2/3} (d_d / l). \tag{39}$$

Here Le is the Lewis number, n_T the total number of the fuel droplets, and l the mean distance between the fuel droplets.

For a numerical approximation of the gas phase, discretization of the nonlinear terms of the momentum equations is derived from a second-order

fully conservative finite difference scheme [49, 50], while those of the scalars such as enthalpy and mass fractions are computed by the QUICK scheme [51]. Other differentials are approximated by a second-order finite difference method. The 3rd-order Runge-Kutta method is used as the time advancement of the calculation of the convective terms. The fractional step method [52] is used as the computational algorithm. On all six boundaries, the free outflow condition is given.

The values of the droplet density, ρ_d, and the specific heat of the droplet, $c_{p,d}$, are calculated by the curve fit data from the NIST web book [44], and other thermo physical properties and transport coefficients under various pressures are obtained from CHEMKIN [53, 54]. Here the reference temperature, T_{ref}, and reference mass fraction, $Y_{k,ref}$, are calculated by "1/3 rule" [26] as

$$T_{ref} = \frac{1}{3}T + \frac{2}{3}T_d,\ Y_{k,ref} = \frac{1}{3}Y_k + \frac{2}{3}Y_{k,s}. \tag{40}$$

Regarding the computations for the evaporation of a single droplet, the droplet diameter of 700 μm is larger than the computational grid, so that PSI-Cell method can not be used. Therefore, the evaporation rate of the single droplet is calculated under the assumption that the variations of the gas temperature and mass fraction of fuel gas caused by the droplet evaporation are negligible small.

3. Results and discussion

3.1. Evaporation of a single fuel droplet without combustion reaction

In this section, the effects of ambient pressure and initial gas temperature on the evaporation of a single fuel droplet are investigated by comparing

with the experiments by Nomura and Ujiie [28]. In the previous numerical study by Yang and Wong [29], they pointed out that radiation from the furnace wall and heat conduction from a fiber used for suspending a fuel droplet may enhance the droplet evaporation in the experiments. In addition, we speculate that natural convection around the droplet surface affects the droplet evaporation. This is because the gravity fluctuation with 1/100 of normal gravity was measured in the experiments, although the experiments were reported to be performed in a micro-gravity condition.

In Fig.3, the comparisons of time variation of normalized squared droplet diameter, $(d/d_0)^2$, between numerical simulations and experiments [28] with and without radiation and natural convection is shown for n-heptane. Here both axises are normalized by the square of the initial droplet diameter. The left-hand side and right-hand side figures show the low-initial-gas-temperature and high-initial-gas-temperature cases, respectively. The radiative heat absorption, Q_{rad}, is calculated as

$$Q_{rad} = \pi d_d^2 \sigma \epsilon (T^4 - T_d^4), \tag{41}$$

where σ is the Stephan-Boltzmann coefficient and ϵ the surface absorptance given by 0.93 [29]. In order to take the effect of the natural convection into account, gravity effect is introduced into the Nusselt and Sherwood numbers as

$$Nu = 2 + 0.6(Gr^{1/2} + Re_{sl})^{1/2} Pr^{1/3}, \tag{42}$$

$$Sh = 2 + 0.6(Gr^{1/2} + Re_{sl})^{1/2} Sc^{1/3}. \tag{43}$$

Here Gr is Grashof number defines as

$$Gr = \frac{g\rho^2 (T - T_d) d_d^3}{T\mu^2}, \tag{44}$$

[55, 56], where g is the gravity. The effect of heat conduction of a fiber used for suspending a fuel droplet is neglected here because of the uncertainty of its condition in the experiments [28]. It is observed that the predictions of $(d/d_0)^2$ monotonously decrease with increasing t/d_0^2 and that their slopes become gentle at low-initial-gas-temperature cases and steep at high-initial-gas-temperature cases as the ambient pressure increases, and become steep as the initial gas temperature increases. Also, the predictions become to be in better agreement with the experiments [28] by taking the effects of the radiation and natural convection into account. In the conditions of high ambient pressure and initial gas temperature (see the right-hand side figure in Fig.3 (c)), however, the differences between the predictions and the experiments are still marked even if the effects of the radiation and natural convection are taken account of. In particular, the effect of the ambient pressure is quite different. Compared to the experiments [28], the increase of droplet size due to droplet expansion greatly surpasses the decrease of it due to droplet evaporation in these conditions in the numerical simulations. It is considered that this is due to the fact that the effect of heat conduction from a fiber used for suspending a fuel droplet, which could enhance the droplet evaporation, is neglected in the numerical simulations. In addition, the difficulties in measuring the droplet size in the experiments may deteriorate the accuracies of the experimental data. The time variations of normalized squared droplet diameter, $(d/d_0)^2$, for n-decane are also shown in Fig.4. In all conditions, the droplet expansion is more evident and the droplet evaporation proceeds slower for n-decane than those for n-heptane.

In the computations for the evaporation and combustion reaction of mul-

tiple fuel droplets, whose results are shown in the following sections, the effects of radiation and natural convection are neglected. This is because small droplets with diameter of 7.5 μm are used so that their evaporation time are very short of a few dozens of μs.

3.2. Evaporation of multiple fuel droplets without combustion reaction

Figs.5 and 6 show the time variations of total droplets' mass, m/m_0, in nitrogen at initial gas temperatures of $T_0 = 1000$, 1500 and 2000 K for $ML =$ 0.027 and 0.12, respectively. As the ambient pressure increases, the start-up of droplet evaporation is delayed and the evaporation rate is enhanced once the evaporation starts. This is because as the ambient pressure increases, droplet evaporation is suppressed by higher boiling temperature because the heat from the ambient gas is used not for evaporation but for raising the droplet temperature, whereas it is enhanced by lower latent heat (see Eq. (26)) and larger droplet surface area due to greater liquid expansion (i.e., lower liquid density) caused by the increase of droplet temperature. The former and latter factors affect the droplet evaporation rate in the early and subsequent evaporation periods, respectively. Also, since only the latter factor is influenced by the ambient gas temperature, the slope of m/m_0 becomes steep with increasing the initial gas temperature, T_0. The comparison of Figs.5 and 6 suggests that this tendency is not influenced by ML.

In order to understand the general effects of the ambient pressure, initial gas temperature and mass loading ratio, ML, on the droplet evaporation, droplet lifetime which is defined as the time when m/m_0 becomes 1% is introduced. Fig.7 shows the effects of ambient pressure, P, and ML on droplet lifetime in nitrogen at initial gas temperatures of $T_0 = 1000$, 1500 and 2000 K.

The droplet lifetime is found to increase with increasing the ambient pressure at lower initial gas temperature of T_0=1000 K, but decrease at higher initial gas temperatures of T_0=1500 and 2000 K. This is attributed to a balance of the increase and decrease of the droplet evaporation rate in higher ambient pressure conditions, as mentioned earlier on Figs. 5 and 6. This tendency is not influenced by ML, but the droplet lifetime quantitatively becomes longer with increasing ML. This is explained by Fig.8 in which the time variations of gas temperature, T, and ratio of mass fraction of evaporated fuel to vapor surface mass fraction, $Y_F/Y_{F,s}$, in nitrogen at initial gas temperature of T_0=2000 K and ambient pressure of P=2.0 MPa (see Fig.7(c)) are shown. Compared to in the case of ML=0.027, the decrease of T and the increase of $Y_F/Y_{F,s}$ with time in the case of ML=0.12 are remarkable, which act to suppress the droplet evaporation and therefore enlarge the droplet lifetime.

Fig.9 shows the effect of inhomogeneity of droplet distribution on droplet lifetime in nitrogen at initial gas temperature of T_0=2000 K for ML=0.027 (without parcel model) and ML=0.054 (with parcel model). In both cases of ML=0.027 and 0.054, the inhomogeneity of droplet distribution is found to make the droplet lifetime longer regardless of the ambient pressure. In order to elucidate the mechanism, probability density function (PDF) of local mass loading ratio, ML_{local}, which is calculated by counting the number of fuel droplets in a cube 0.5 mm on a side, is evaluated at ambient pressure of P=2.0 MPa as shown in Fig.10. Compared to the random droplet distribution, the PDF of the inhomogeneous droplet distribution widely distributes in the higher ML_{local} region, which is considered to contribute to the longer droplet lifetime.

3.3. Evaporation of multiple fuel droplets with combustion reaction

Figs.11 and 12 show the time variations of distributions of instantaneous gas temperature, T, mass fraction of O_2, Y_{O_2}, and mass fraction of fuel gas, Y_F, in air at initial gas temperature of T_0=2000 K, ambient pressure of P=0.1 MPa, and ML=0.12 and 0.36, respectively. These conditions are ones in Cases 14 and 15 and indicate the Group combustion number (see Eq. (39)) of G=6.8 and 20.4, respectively. It is observed that although the tendencies that Y_{O_2} and Y_F decreases and increases, respectively, in the central region with time are similar between the cases of ML=0.12 and 0.36, the distributions of T are considerably different. This difference is considered to be in the combustion form, as known as "droplet group combustion". According to Chiu and Liu [57] and Chiu et al. [58], there are four modes in the droplet group combustion of spray flames, i.e., (1) single droplet combustion mode in which all droplets burn with envelope flames, (2) internal group combustion mode in which the group flame appears inside the droplet group (droplets inside the group flame only just evaporate and droplets outside the group flame burn with envelope flames), (3) external group combustion mode in which the group flame encloses the whole droplet group, and (4) external sheath combustion mode in which the nonevaporation region (low temperature region) is found inside the evaporation region in the droplet group. These modes change from the single droplet combustion mode to the external sheath combustion mode, as the group combustion number, G, increases. Judging from this concept, the combustion behaviors in both cases of ML=0.12 and 0.36 for P=0.1 MPa are considered to be classified into the mode (3), but they seem to be classified into the modes (2) and (3),

respectively, from the viewpoint of the physical phenomena. The similar discrepancies were observed in higher ambient pressure conditions, namely the Chiu's criterion overestimates the group combustion behavior. This is attributed to the fact that the Chiu's criterion does not consider the effect of the initial oxygen concentration in the droplet group [2, 13].

Figs.13, 14 and 15 show the time variations of total droplets' mass, m/m_0 in air at initial gas temperatures of T_0=1000, 1500 and 2000 K for ML=0.027, 0.12 and 0.36, respectively. Regarding the case of ML=0.36, only the results at $T_0 = 2000$ K are shown because the combustion reaction did not take place at T_0=1000 and 1500 K. It is observed that the general tendencies of droplet evaporation are the same as the cases without combustion reaction, namely the start-up of droplet evaporation is delayed and the evaporation rate is enhanced once the evaporation starts as the ambient pressure increases, regardless of the value of ML. However, the droplet evaporation with combustion reaction is faster than that without it. In particular, the droplet evaporation in the cases of higher ambient pressure of $P > 0.1$ MPa are much faster than that in the case of $P = 0.1$ MPa. This is because the increase of the combustion reaction rate with the ambient pressure raises the gas temperature, which enhances the droplet evaporation.

Like the cases without combustion reaction, the effects of ambient pressure, P, and ML on the droplet lifetime in air at initial gas temperatures of $T_0 = 1000$, 1500 and 2000 K are presented in Fig.16. It is verified that the effects of initial gas temperature and ambient pressure on the droplet lifetime are similar to those without combustion reaction, such that the droplet lifetime increases with increasing the ambient pressure at lower initial gas

temperature of 1000 K, but decreases at higher initial gas temperatures of 1500 K and 2000 K. On the other hand, the effect of ML on the droplet lifetime is somewhat complicated. That is, the increase of ML increases the droplet lifetime at $T_0 = 1000$ K, decreases it at $T_0 = 1500$ K, and changes the effect depending on ML (i.e., decreases the droplet lifetime at moderately high ML and conversely increases it at higher ML) at $T_0 = 2000$ K. This is explained by Fig.17 in which the time variations of gas temperature, T, and ratio of mass fraction of evaporated fuel to vapor surface mass fraction, $Y_F/Y_{F,s}$, in air at initial gas temperature of T_0=2000 K and ambient pressure of P=2.0 MPa (see Fig.16(c)) are shown. It is found that as ML increases, T becomes to rise quickly and $Y_F/Y_{F,s}$ monotonously increases. The trend of T, which is caused by the enhancement of the combustion reaction, is quite different between the cases with and without combustion reaction, while that of $Y_F/Y_{F,s}$ is similar. Here the increases of T and $Y_F/Y_{F,s}$ act to enhance and suppress the droplet evaporation, namely shorten and enlarge the droplet lifetime, respectively. Accordingly, it can be said that the effect of ML on the droplet lifetime is determined by a balance of the increases of T and $Y_F/Y_{F,s}$. Generally speaking, the droplet lifetime tends to be lengthened by the increase of ML even under the condition with combustion reaction, but often shortened at moderately high ML at high ambient pressure.

Fig.18 shows the effect of inhomogeneity of droplet distribution on droplet lifetime in air at initial gas temperature of T_0=2000 K for ML=0.027 (without parcel model) and ML=0.054 (with parcel model). In the cases of ML=0.054, the inhomogeneity of droplet distribution is found to make the droplet lifetime longer regardless of the ambient pressure. In the cases of

ML=0.027, on the other hand, the inhomogeneity of droplet distribution does not always make the droplet lifetime longer. This is due to the same reasons, as mentioned above, that is, the droplet lifetime is shortened by moderately high ML.

4. Conclusions

In this study, the effects of ambient pressure, initial gas temperature and combustion reaction on the evaporation of a single fuel droplet and multiple fuel droplets were investigated by means of three-dimensional numerical simulation. The ambient pressure, initial gas temperature and mass loading ratio, ML, were varied in the ranges of 0.1-2.0 MPa, 1000-2000 K and 0.027-0.36, respectively, under the condition with or without combustion reaction. The main results obtained in this study can be summarized as follows.

1. Natural convection accelerates droplet evaporation, and the effect becomes remarkable with increasing the ambient pressure.
2. Under the condition without combustion reaction, droplet lifetime increases with increasing the ambient pressure at lower initial gas temperature of 1000 K, but decreases at higher initial gas temperatures of 1500 K and 2000 K. This is attributed to a balance of the increase and decrease of droplet evaporation rate in higher ambient pressure conditions. Namely, as the ambient pressure increases, droplet evaporation is suppressed by higher boiling temperature, whereas it is enhanced by lower latent heat and larger droplet surface due to greater liquid expansion caused by the increase of droplet temperature. This tendency is not influenced by ML, but the droplet lifetime quantitatively becomes

longer with increasing ML because of the decrease of gas temperature and the increase of the evaporated fuel mass fraction towards the vapor surface mass fraction.

3. The effects of ambient pressure, initial gas temperature and ML on the droplet lifetime under the condition with combustion reaction are similar to those under the condition without combustion reaction, although the droplet lifetime becomes shorter due to the combustion reaction. However, the droplet lifetime is often shortened by enhanced combustion reaction in the conditions of high ambient pressure and moderately high ML.
4. Both for the conditions with and without combustion reaction, inhomogeneity of droplet distribution caused by turbulence makes the droplet lifetime longer because local ML dramatically increases in some locations.

Acknowledgments

The authors are grateful to Dr. Hiroaki Watanabe of Central Research Institute of Electric Power Industry (CRIEPI) for many useful discussions. This research was partially supported by "Strategic Programs for Innovative Research (SPIRE) - Field No. 4: Industrial Innovations" from MEXT (Ministry of Education, Culture, Sports, Science, and Technology).

References

[1] C. S. Cooper, N. M. Laurendeau, Combust. Flame 123 (2000) 175-188.

[2] M. Nakamura, F. Akamatsu, R. Kurose, M. Katsuki, Phys. Fluids 17 (2005) 123301.

[3] P. Domingo, L. Vervisch, J. Réveillon, Combust. Flame 140 (2005) 172-195.

[4] J. Réveillon, L. Vervisch, J. Fluid Mech. 537 (2005) 317-347.

[5] H. Watanabe, R. Kurose, S.-M. Hwang, F. Akamatsu, Combust. Flame 148 (2007) 234-248.

[6] H. Watanabe, R. Kurose, S. Komori, H. Pitsch, Combust. Flame 152 (2008) 2-13.

[7] Y. Baba, R. Kurose, J. Fluid Mech. 612 (2008) 45-79.

[8] A. Neophytou, E. Mastorakos, R. S. Cant, Combust. Flame 157 (2010) 1071-1086.

[9] J. Hayashi, H. Watanabe, R. Kurose, F. Akamatsu, Combust. Flame 158 (2011) 2559-2568.

[10] K. Luo, H. Pitsch, M. G. Pai, O. Desjardins, Proc. Combust. Inst. 33 (2011) 2143-2152.

[11] A. Fujita, H. Watanabe, R. Kurose, S. Komori, Fuel 104 (2013) 515-525.

[12] T. Kitano, T. Nakatani, R. Kurose, S. Komori, Fuel 104 (2013) 526-535.

[13] K. Hagihara, H. Yamashita, K. Yamamoto, J. Combust. Soc. Japan 51 (2009) 343-353 (In Japanese).

[14] P. Schroll, A. P. Wandel, R. S. Cant, E. Mastorakos, Proc. Combust. Inst. 32 (2009) 2275-2282.

[15] A. Neophytou, E. Mastorakos, R. S. Cant, Proc. Combust. Inst. 33 (2011) 2135-2142.

[16] M. L. Botero, Y. Huang, D. L. Zhu, A. Molina, C. K. Law, Fuel 94 (2012) 342-347.

[17] G. Borghesi, E. Mastorakos, R. S. Cant, Combust. Flame 160 (2013) 1254-1274.

[18] P. Moin, S. V. Apte, AIAA J. 44 (2006) 698-708.

[19] M. Boileau, S. Pascaud, E. Riber, B. Cuenot, L. Y. M. Gicquel, T. J. Poinsot, M. Cazalens, Flow Turb. Combust. 80 (2008) 291-321.

[20] N. Patel, S. Menon, Combust. Flame 153 (2008) 228-257.

[21] M. Ihme, H. Pitsch, Phys. Fluids 20 (2008) 055110.

[22] H. Moriai, R. Kurose, H. Watanabe, Y. Yano, F. Akamatsu, S. Komori, J. Eng. Gas Turbines Power 135 (2013) 091503.

[23] S. Russo, A. Gomez, Combust. Flame 145 (2006) 339-356.

[24] R. Ryser, T. Gerber, T. Dreier, Combust. Flame 156 (2009) 120-129.

[25] M. Nakamura, D. Nishioka, J. Hayashi, F. Akamatsu, Combust. Flame 158 (2011) 1615-1623.

[26] R. S. Miller, K. Harstad, J. Bellan, Int. J. Multiphase Flow 24 (1998) 1025-1055.

[27] R. S. Miller, J. Bellan, J. Fluid Mech. 384 (1999) 293-338.

[28] H. Nomura, Y. Ujiie, Proc. Combust. Inst. 26 (1996) 1267-1273.

[29] J.-R. Yang, S.-C. Wong, Int. J. Heat Mass Transfer 44 (2001) 4433-4443.

[30] K. Harstad, J. Bellan, Int. J. Multiphase Flow 26 (2000) 1675-1706.

[31] M. Mikami, M. Kono, J. Sato, D. L. Dietrich, Proc. Combust. Inst. 27 (1998) 2643-2649.

[32] C. T. Crowe, M. P. Sharma, D. E. Stock, Trans. ASME J. Fluid. Eng. 99 (1977) 325-332.

[33] J. Bellan, K. Harstad, Int. J. Heat Mass Transfer 30 (1987) 125-136.

[34] R. Kurose, H. Makino, S. Komori, M. Nakamura, F. Akamatsu, M. Katsuki, Phys. Fluids 15 (2003) 2338-2351.

[35] S. S. Sazhin, Prog. Energy Combust. Sci. 32 (2006) 162-214.

[36] S. Tonini, G. E. Cossali, Int. J. Thermal Sci. 57 (2012) 45-53.

[37] C. Maqua, G. Castanet, F. Grisch, F. Lemoine, T. Kristyadi, S. S. Sazhin, Int. J. Heat Mass Transfer 51 (2008) 3932-3945.

[38] S. S. Sazhin, J.-F. Xie, I. N. Shishkova, A. E. Elwardany, M. R. Heikal, Int. J. Heat Mass Transfer 56 (2013) 525-537.

[39] S. S. Sazhin, T. Kristyadi, W. A. Abdelghaffar, M. R. Heikal, Fuel 85 (2006) 1613-1630.

[40] K. Sato, Estimation of Physical Property Coefficients, Maruzen Publishing Co., Ltd, Japan, 1954 (In Japanese).

[41] K. M. Watson, Ind. Eng. Chem. 35 (1943) 398-406.

[42] D. Y. Peng, D. B. Robinson, Ind. Eng. Chem. Fundam. 15 (1976) 59-64.

[43] R. D. Gunn, T. Yamada, AIChE J. 17 (1971) 1341-1345.

[44] NIST 2011 http://webbook.nist.gov/chemistry/ In NIST Chemistry WebBook, NIST Standard Reference Database (ed. P. J. Linstrom, W. G. Mallard)

[45] C. B. Willingham, W. J. Taylor, J. M. Pignocco, F. D. Rossini, J. Res. National Bureau Stand. 35 (1945) 219-244.

[46] C. K. Westbrook, F. L. Dryer, Prog. Energy Combust. Sci. 10 (1984) 1-57.

[47] K. Matsuda, R. Onishi, R. Kurose, S. Komori, Phys. Rev. Lett. 108 (2012) 224502.

[48] F. Akamatsu, Y. Mizutani, M. Katsuki, S. Tsushima, Y. D. Cho, Proc. Combust. Inst. 26 (1996) 1723-1729.

[49] Y. Morinishi, T. S. Lund, O. V. Vasilyev, P. Moin, J. Comp. Phys. 143 (1998) 90-124.

[50] F. Nicoud, J. Comp. Phys. 158 (2000) 71-97.

[51] A. Leonard, Comp. Meth. Appl. Mech. Eng. 19 (1979) 59-98.

[52] V. Moureau, C. Berat, H. Pitsch, J. Comp, Phys. 226 (2007) 1256-1270.

[53] R. J. Kee, G. Dixon-Lewis, J. Warnaz, M. E. Coltrin, J. A. Miller, Sandia Report (1986) SAND86-8246.

[54] R. J. Kee, F. M. Rupley, J. A. Miller, Sandia Report (1989) SAND89-8009B.

[55] E. W. Curtis, P. V. Farrell, Combust. Flame 90 (1992) 85-102.

[56] W. E. Ranz, W. R. Marshall, Chem. Eng. Prog. 48 (1952) 141-146.

[57] H. H. Chiu and T. M. Liu, Combust. Sci. Technol. 17 (1977) 127-142.

[58] H. H. Chiu, H. Y. Kim, E. J. Croke, Proc. Combust. Inst. 19 (1982) 971-980.

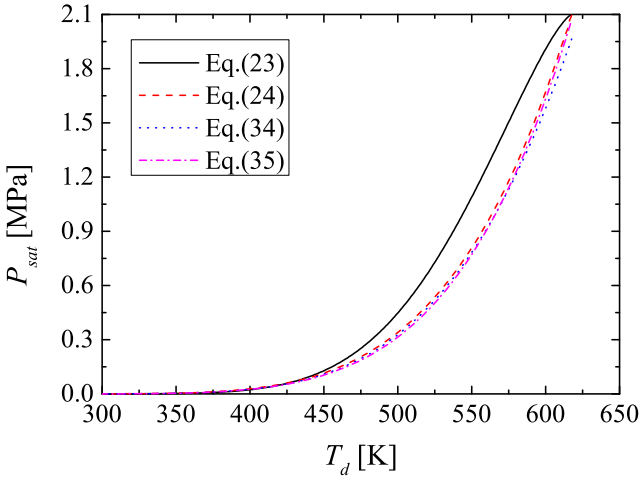

(a) n-decane

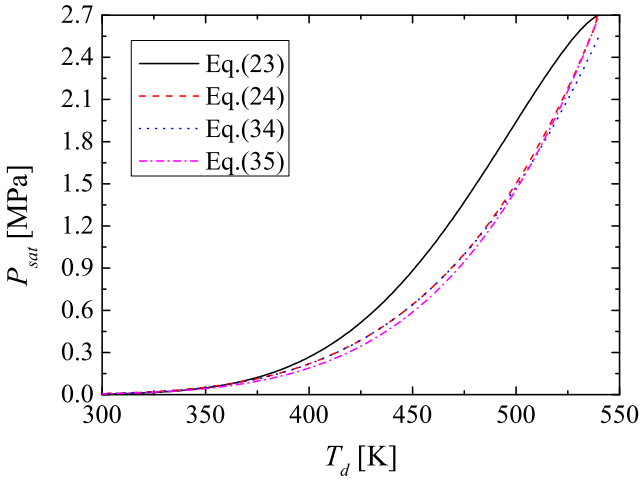

(b) n-heptane

Figure 1: Comparison of saturated vapor pressure, P_{sat}, against droplet surface temperature, T_d, calculated by Eqs.(23),(24),(34) and (35) for (a) n-decane and (b) n-heptane.

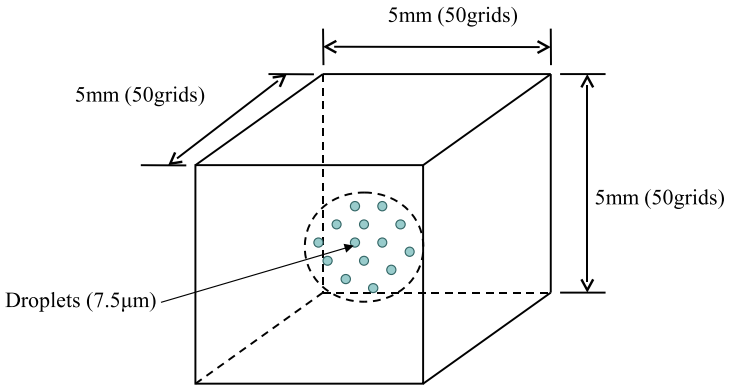

(a) Computational domain

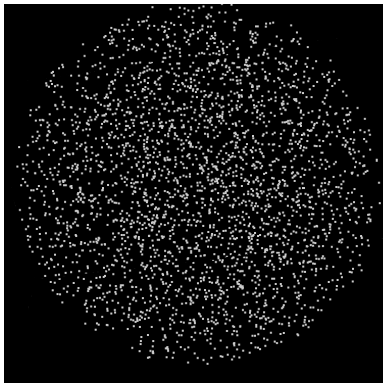

(b) Random distribution

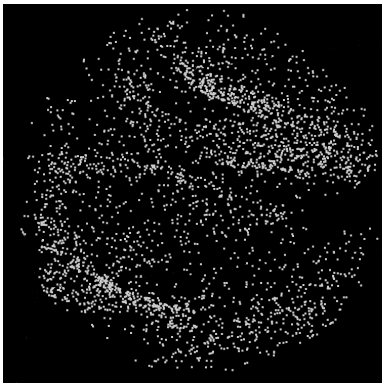

(c) Inhomogeneous distribution by turbulence

Figure 2: Computational domain and initial droplet distributions.

Table 1: Cases and computational conditions.

Cases	P [MPa]	T_0 [K]	ML [-] (ϕ [-])	Ambient gas	Droplet distribution	G [-]
1	0.1 - 2.0	1000	0.027 (-)	nitrogen	random	2.8-61.8
2	0.1 - 2.0	1500	0.027 (-)	nitrogen	random	2.1-46.4
3	0.1 - 2.0	2000	0.027 (-)	nitrogen	random	1.4-30.9
4*	0.1 - 2.0	2000	0.054 (-)	nitrogen	random	2.8-61.8
5	0.1 - 2.0	1000	0.12 (-)	nitrogen	random	13.6-276.0
6	0.1 - 2.0	1500	0.12 (-)	nitrogen	random	10.2-207.0
7	0.1 - 2.0	2000	0.12 (-)	nitrogen	random	6.8-138.0
8	0.1 - 2.0	1000	0.027 (0.411)	air	random	2.8-61.8
9	0.1 - 2.0	1500	0.027 (0.411)	air	random	2.1-46.4
10	0.1 - 2.0	2000	0.027 (0.411)	air	random	1.4-30.9
11*	0.1 - 2.0	2000	0.054 (0.822)	air	random	2.8-61.8
12	0.1 - 2.0	1000	0.12 (1.85)	air	random	13.6-276.0
13	0.1 - 2.0	1500	0.12 (1.85)	air	random	10.2-207.0
14	0.1 - 2.0	2000	0.12 (1.85)	air	random	6.8-138.0
15	0.1 - 2.0	2000	0.36 (5.55)	air	random	20.4-414.0
16	0.1 - 2.0	2000	0.027 (-)	nitrogen	inhomogeneous	1.4-30.9
17*	0.1 - 2.0	2000	0.054 (-)	nitrogen	inhomogeneous	2.8-61.8
18	0.1 - 2.0	2000	0.027 (0.411)	air	inhomogeneous	1.4-30.9
19*	0.1 - 2.0	2000	0.054 (0.822)	air	inhomogeneous	2.8-61.8

* Cases using a parcel model in which one parcel represents two fuel droplets.

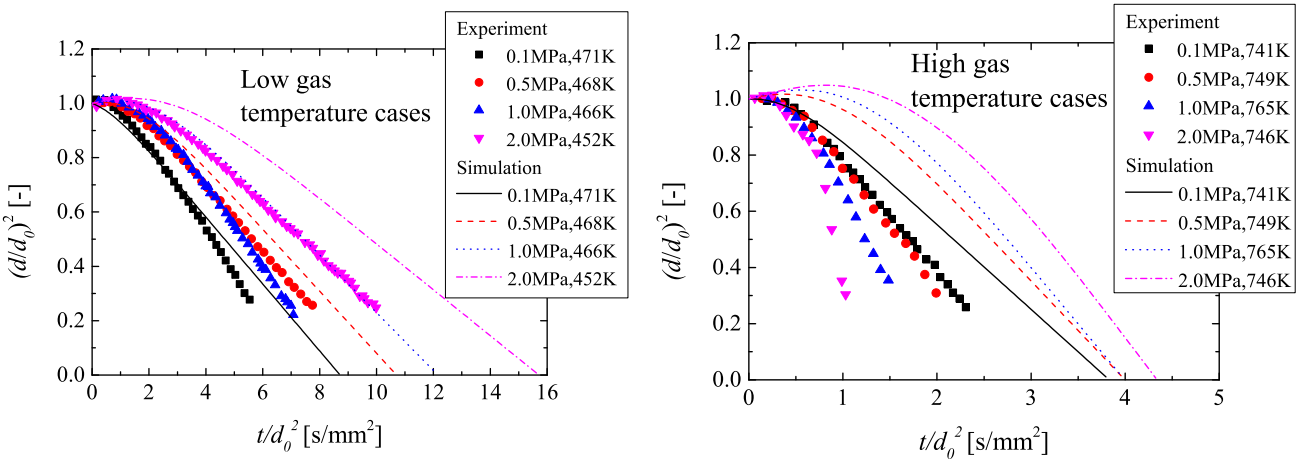

(a) Without radiation and natural convection

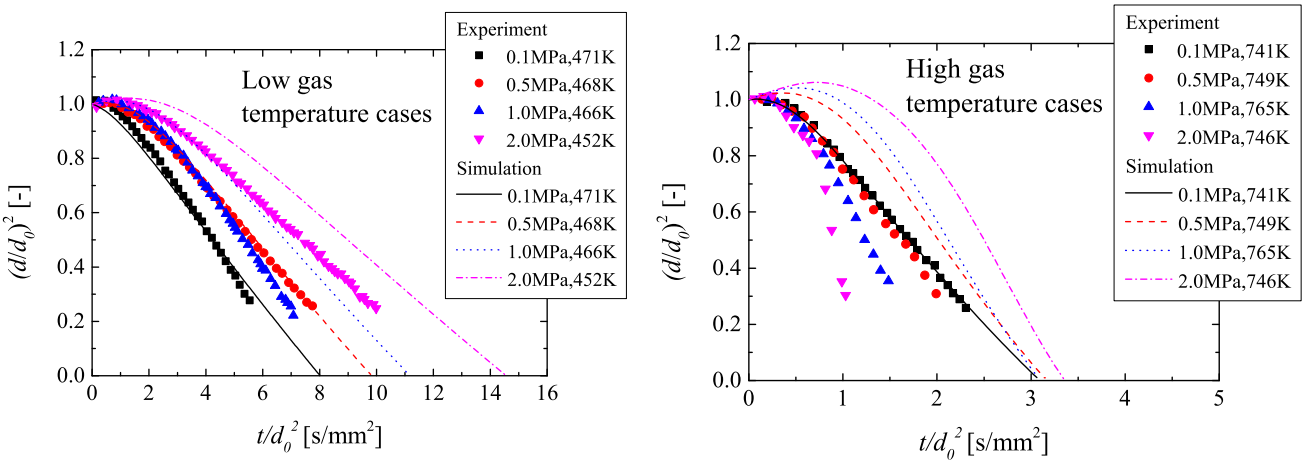

(b) With radiation

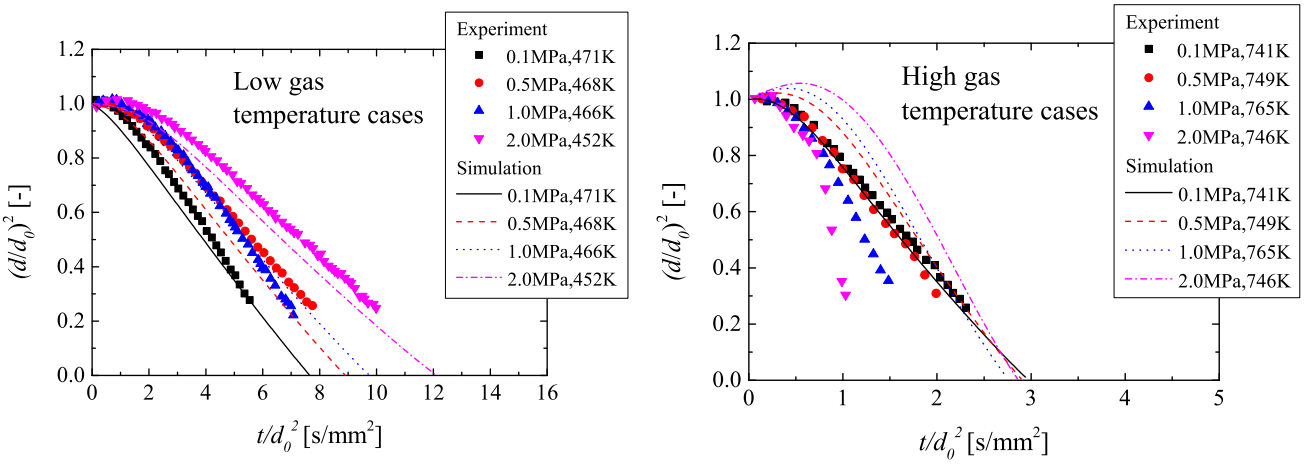

(c) With radiation and natural convection

Figure 3: Comparisons of time variation of normalized squared droplet diameter, $(d/d_0)^2$, between numerical simulations and experiments for n-heptane (a) without radiation and natural convection, (b) with radiation and (c) with radiation and natural convection. Left-hand side shows low-initial-gas-temperature cases and right-hand side shows high-initial-gas-temperature cases.

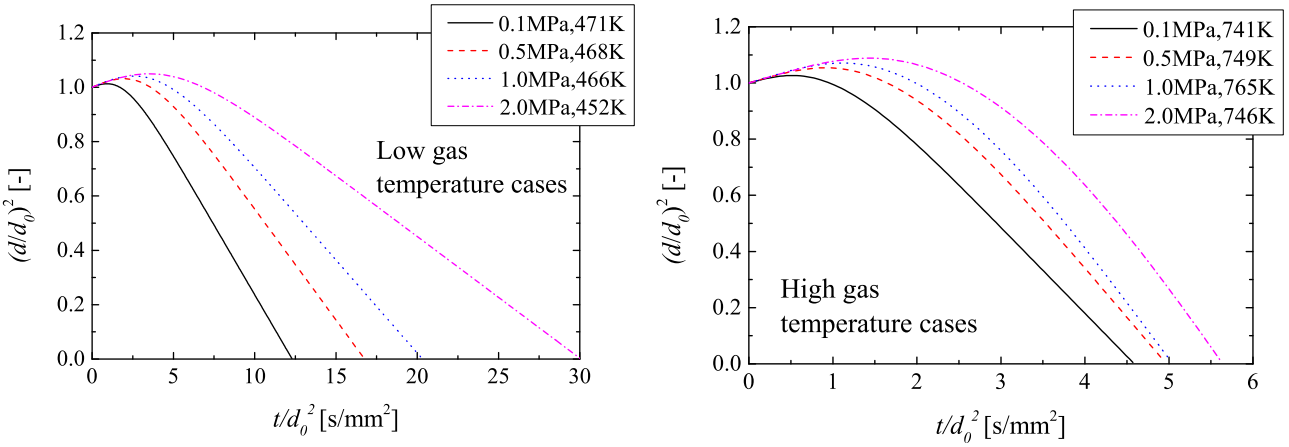

(a) Without radiation and natural convection

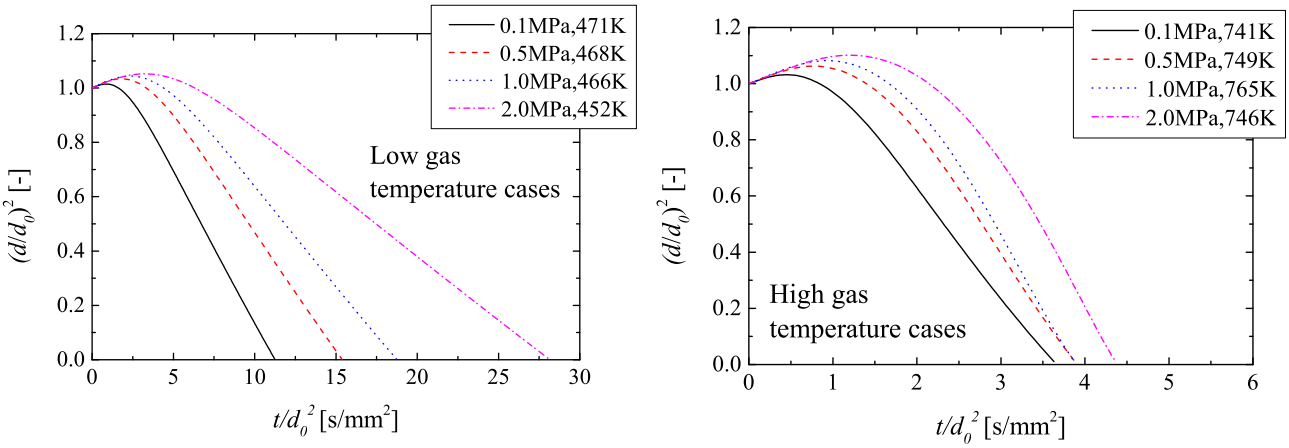

(b) With radiation

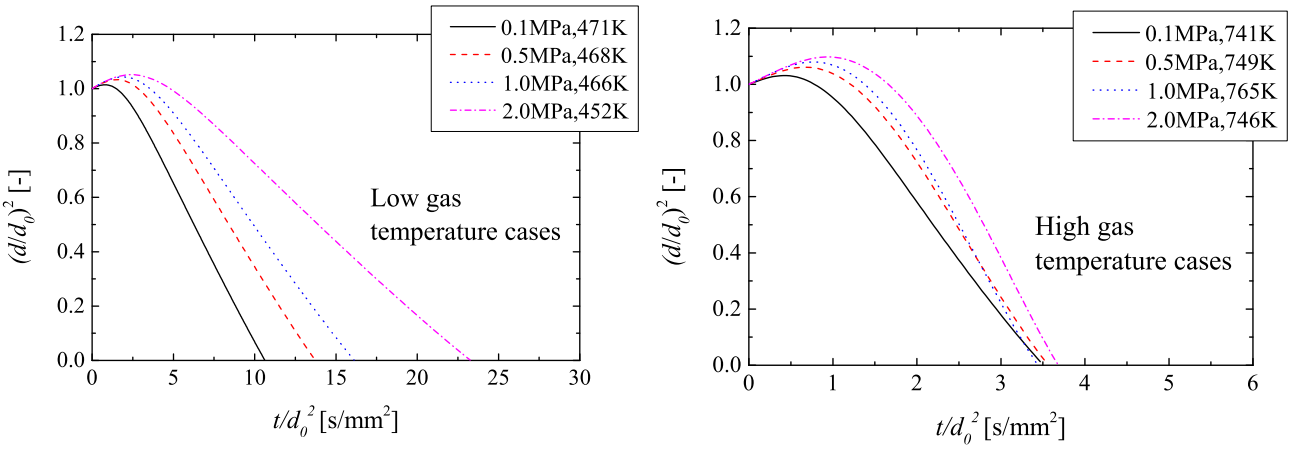

(c) With radiation and natural convection

Figure 4: Time variations of normalized squared droplet diameter, $(d/d_0)^2$, for n-decane (a) without radiation and natural convection, (b) with radiation and (c) with radiation and natural convection. Left-hand side shows low-initial-gas-temperature cases and right-hand side shows high-initial-gas-temperature cases.

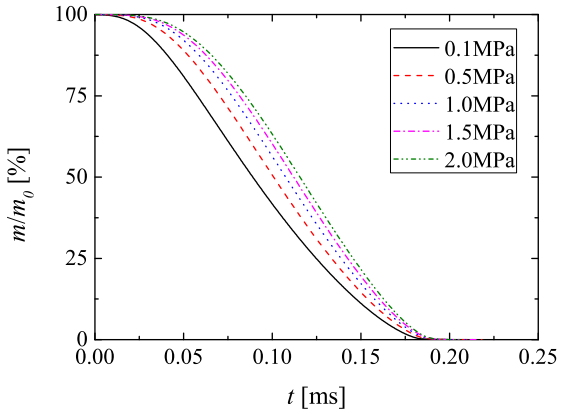

(a) T_0=1000 K (Case 1)

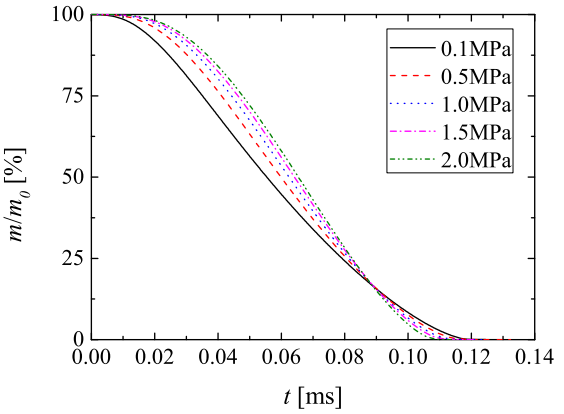

(b) T_0=1500 K (Case 2)

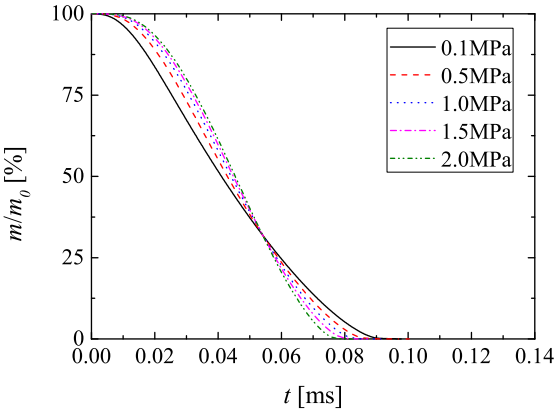

(c) T_0=2000 K (Case 3)

Figure 5: Time variations of total droplets' mass, m/m_0, for ML=0.027 in nitrogen at initial gas temperature of (a) T_0=1000 K, (b) T_0=1500 K and (c) T_0=2000 K.

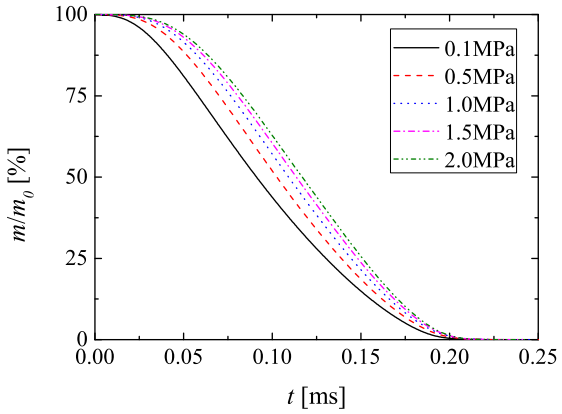

(a) T_0=1000 K (Case 5)

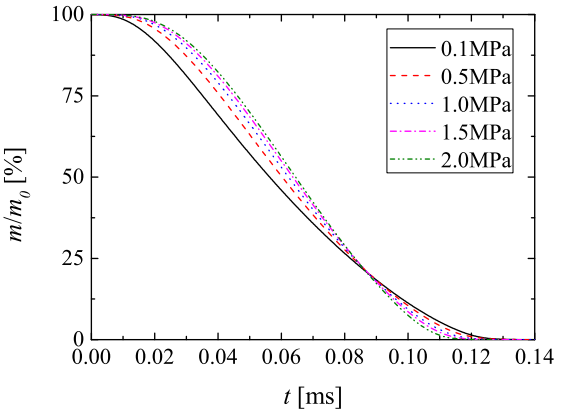

(b) T_0=1500 K (Case 6)

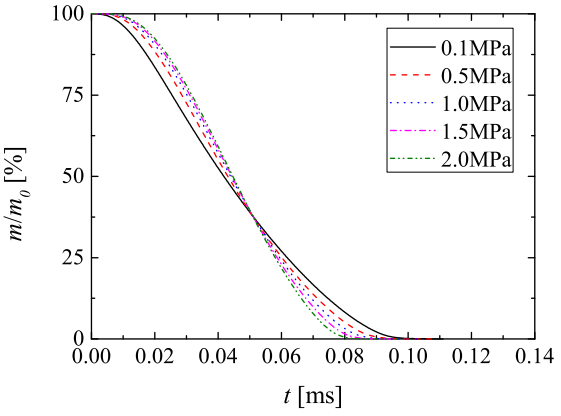

(c) T_0=2000 K (Case 7)

Figure 6: Time variations of total droplets' mass, m/m_0, for ML=0.12 in nitrogen at initial gas temperature of (a) T_0=1000 K, (b) T_0=1500 K and (c) T_0=2000 K.

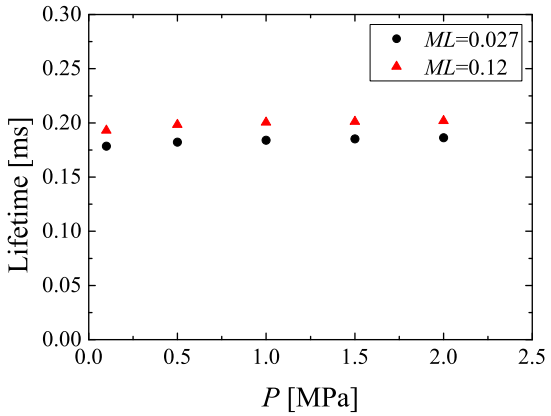

(a) T_0=1000 K (Cases 1 and 5)

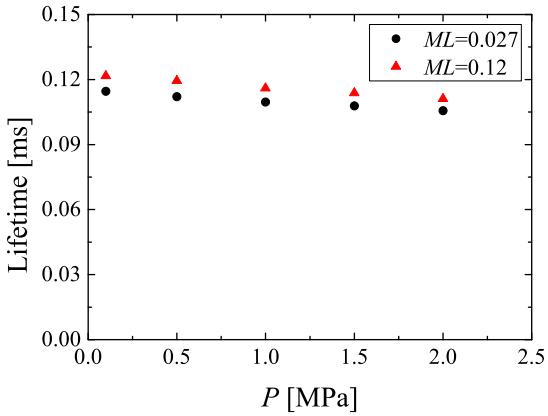

(b) T_0=1500 K (Cases 2 and 6)

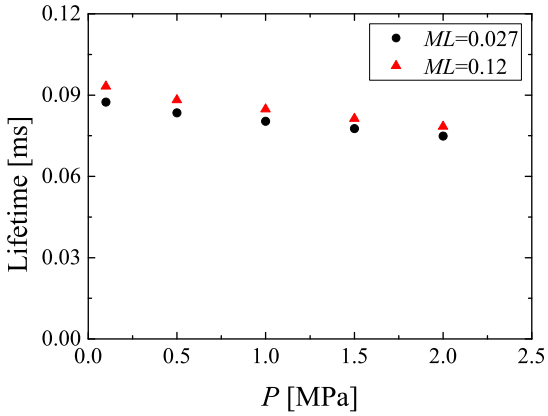

(c) T_0=2000 K (Cases 3 and 7)

Figure 7: Effects of ambient pressure, P, and ML on droplet lifetime in nitrogen at initial gas temperature of (a) T_0=1000 K, (b) T_0=1500 K and (c) T_0=2000 K.

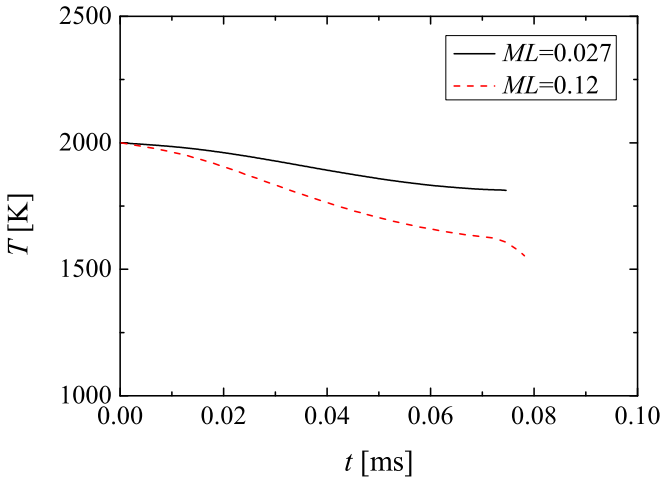

(a) T

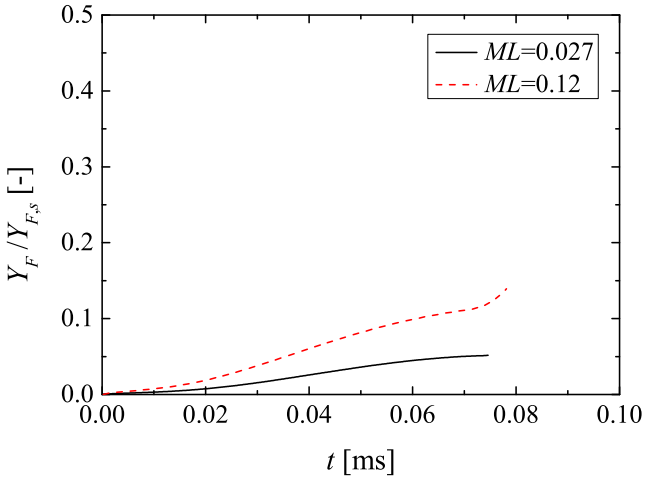

(b) $Y_F/Y_{F,s}$

Figure 8: Time variations of (a) gas temperature, T, and (b) ratio of mass fraction of evaporated fuel to vapor surface mass fraction, $Y_F/Y_{F,s}$, in nitrogen at initial gas temperature of T_0=2000 K and ambient pressure of P=2.0 MPa (see Fig.7 (c)).

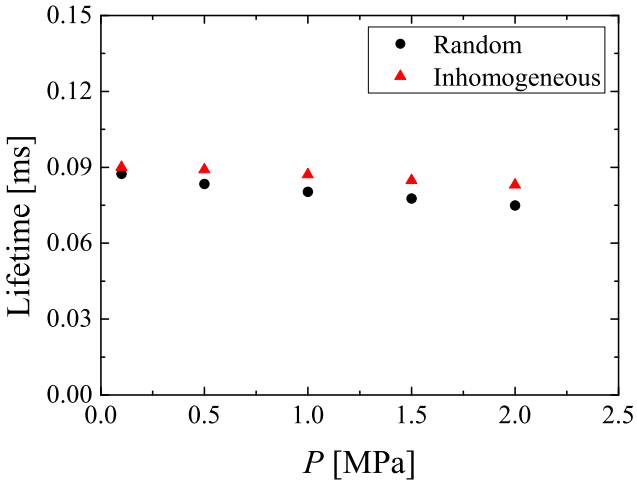

(a) ML=0.027 (without parcel model, Cases 3 and 16)

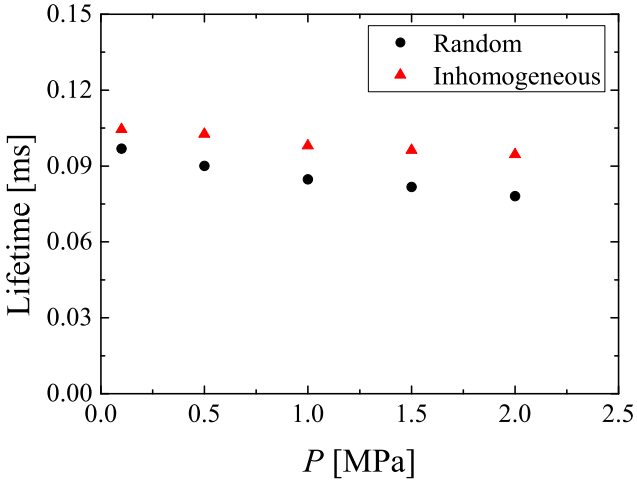

(b) ML=0.054 (with parcel model, Cases 4 and 17)

Figure 9: Effect of inhomogeneity of droplet distribution on droplet lifetime in nitrogen at initial gas temperature of T_0=2000 K for (a) ML=0.027 (without parcel model) and (b) ML=0.054 (with parcel model).

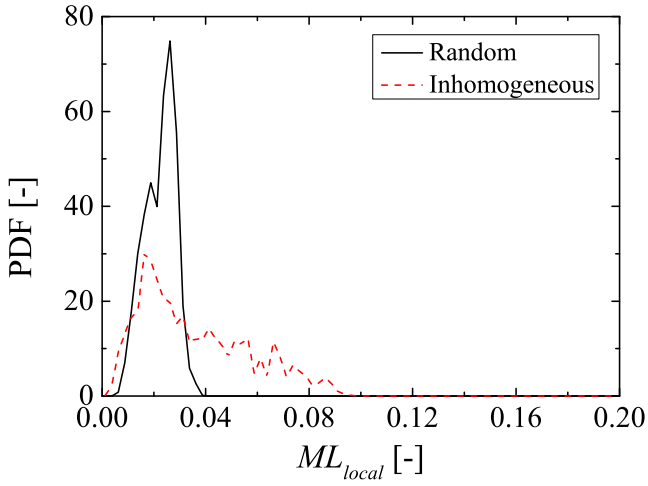

(a) ML=0.027 (without parcel model, Cases 3 and 16)

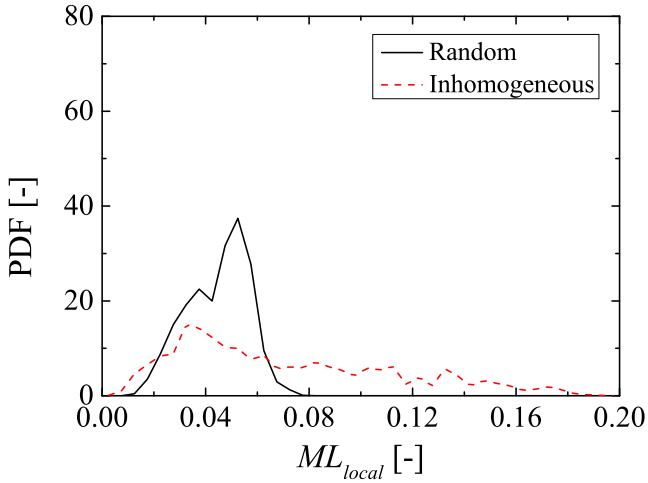

(b) ML=0.054 (with parcel model, Cases 4 and 17)

Figure 10: Effect of inhomogeneity of droplet distribution on PDF of local mass loading ratio, ML_{local}, in nitrogen at initial gas temperature of T_0=2000 K and ambient pressure of P=2.0 MPa for (a) ML=0.027 (without parcel model) and (b) ML=0.054 (with parcel model).

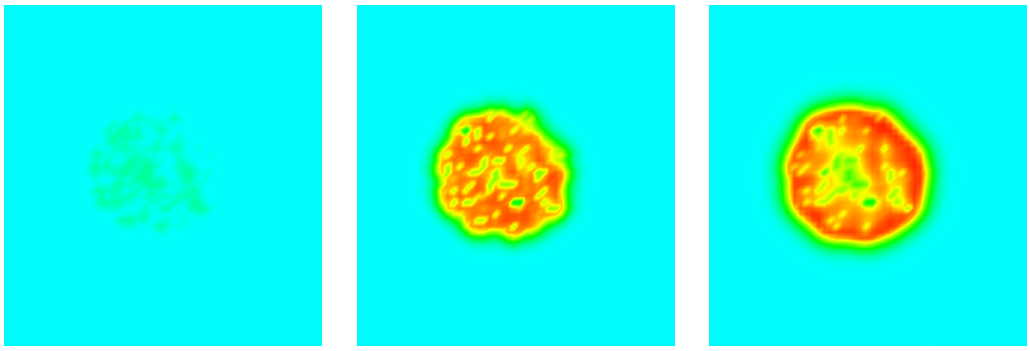

t=10 μs t=30 μs t=50 μs

1500 [K] 3500 [K]

(a) Gas temperature

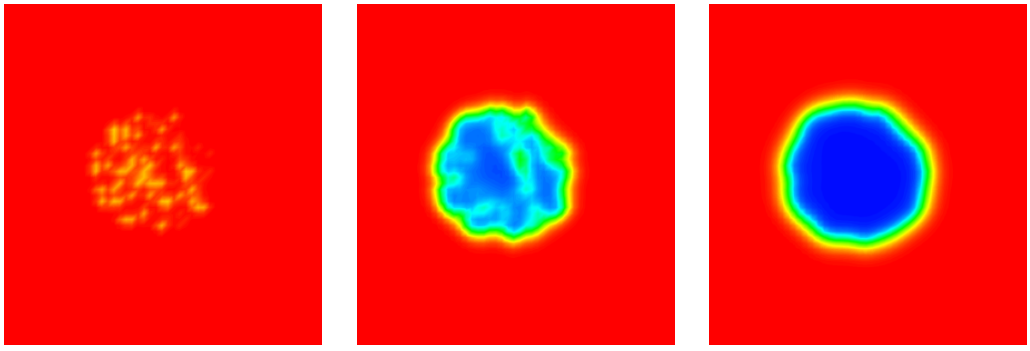

t=10 μs t=30 μs t=50 μs

0 0.23

(b) Mass fraction of O_2

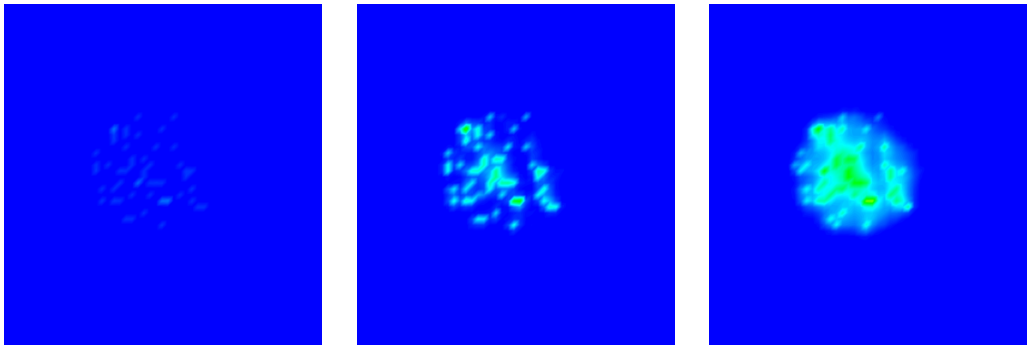

t=10 μs t=30 μs t=50 μs

0 0.3

(c) Mass fraction of fuel gas

Figure 11: Time variations of distributions of instantaneous (a) gas temperature, T, (b) mass fraction of O_2, Y_{O_2}, and (c) mass fraction of fuel gas, Y_F, in air at initial gas temperature of T_0=2000 K, ambient pressure of P=0.1 MPa, and ML=0.12 in Case 14.

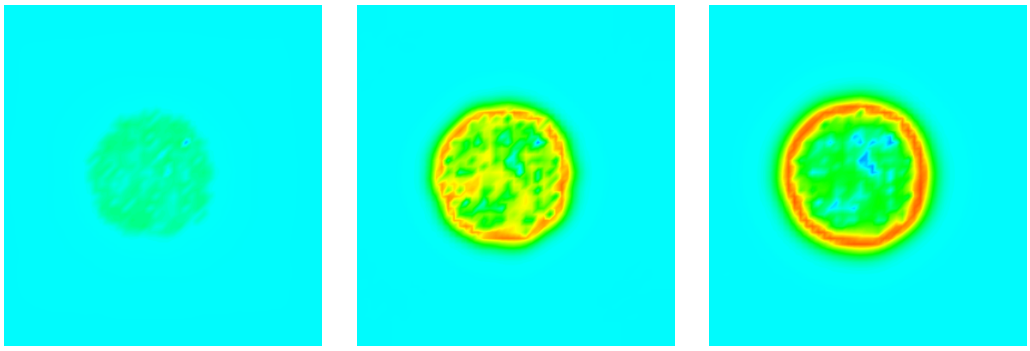

t=10 μs t=30 μs t=50 μs

1500 [K] 3500 [K]

(a) Gas temperature

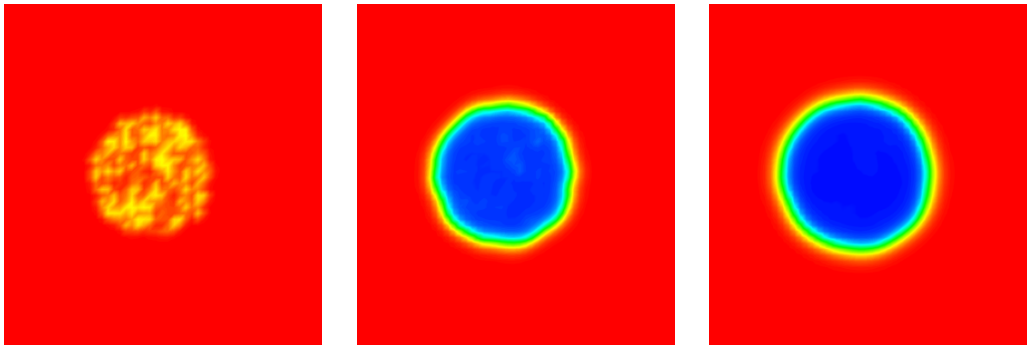

t=10 μs t=30 μs t=50 μs

0 0.23

(b) Mass fraction of O_2

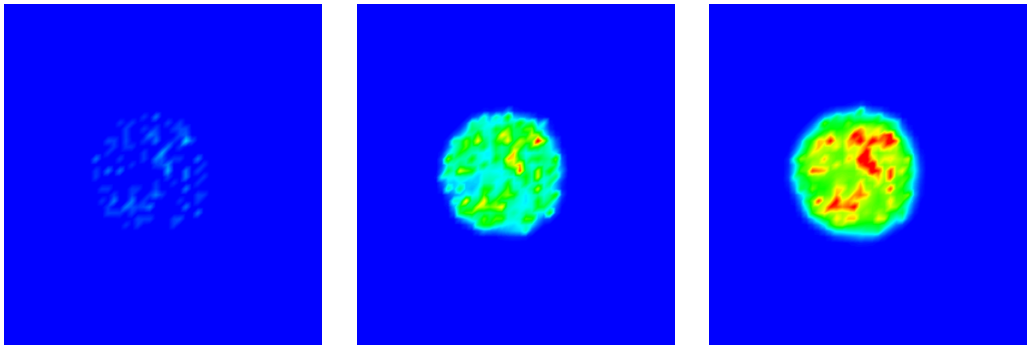

t=10 μs t=30 μs t=50 μs

0 0.3

(c) Mass fraction of fuel gas

Figure 12: Time variations of distributions of instantaneous (a) gas temperature, T, (b) mass fraction of O_2, Y_{O_2}, and (c) mass fraction of fuel gas, Y_F, in air at initial gas temperature of T_0=2000 K, ambient pressure of P=0.1 MPa, and ML=0.36 in Case 15.

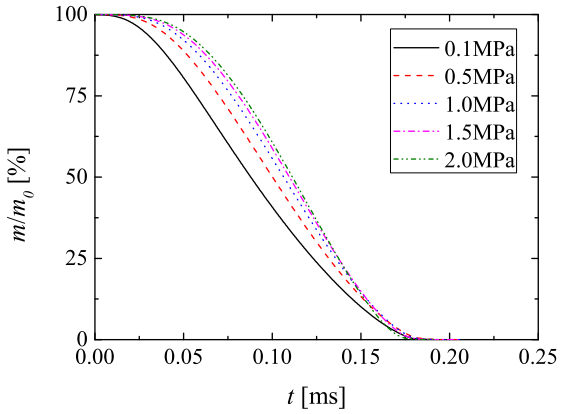

(a) T_0=1000 K (Case 8)

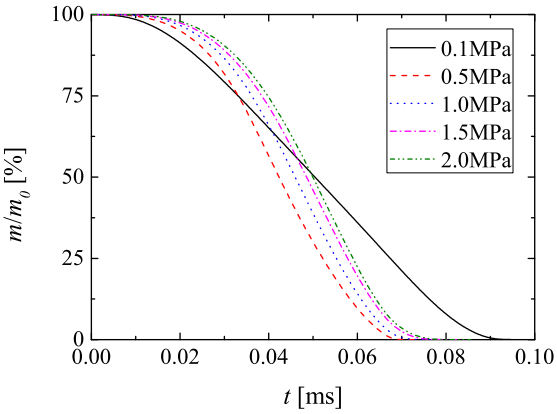

(b) T_0=1500 K (Case 9)

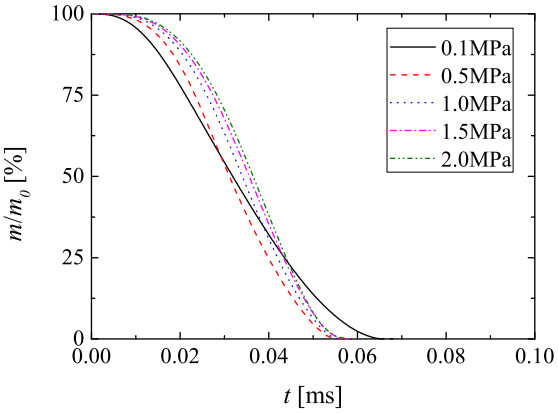

(c) T_0=2000 K (Case 10)

Figure 13: Time variations of total droplets' mass, m/m_0, for ML=0.027 in air at initial gas temperature of (a) T_0=1000 K, (b) T_0=1500 K and (c) T_0=2000 K.

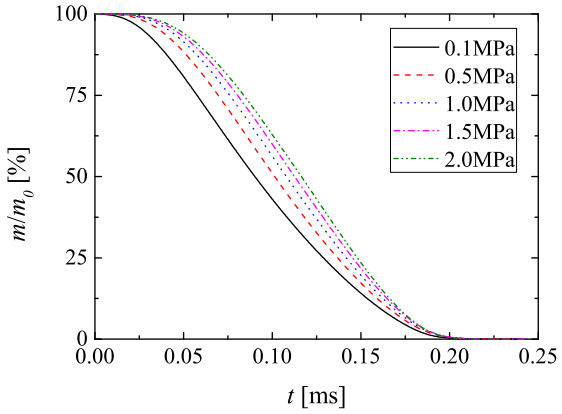

(a) T_0=1000 K (Case 12)

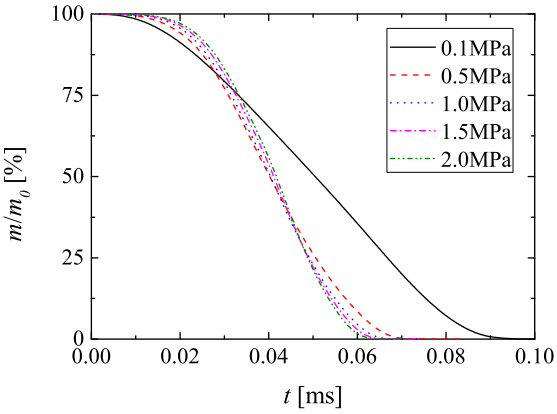

(b) T_0=1500 K (Case 13)

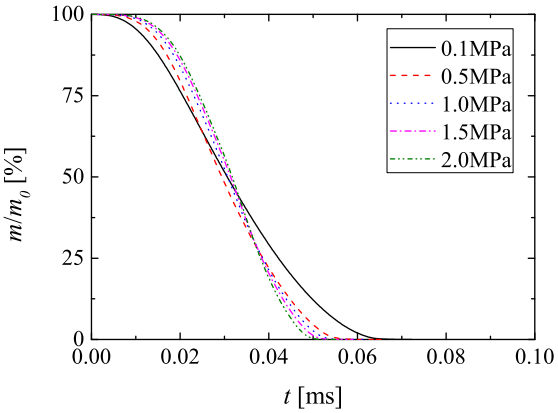

(c) T_0=2000 K (Case 14)

Figure 14: Time variations of total droplets' mass, m/m_0, for ML=0.12 in air at initial gas temperature of (a) T_0=1000 K, (b) T_0=1500 K and (c) T_0=2000 K.

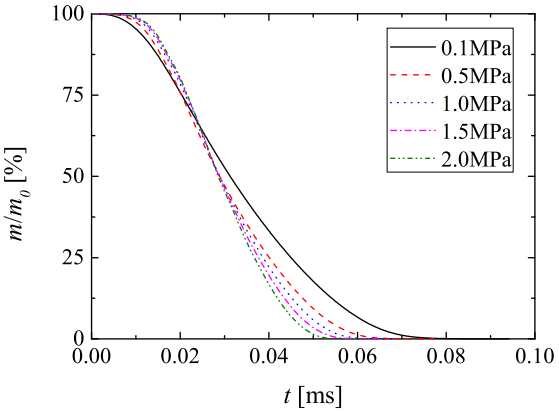

Figure 15: Time variations of total droplets' mass, m/m_0, for ML=0.36 in air at initial gas temperature of T_0=2000 K.

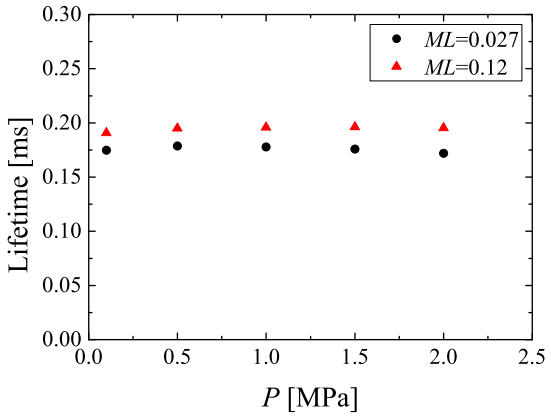

(a) T_0=1000 K (Cases 8 and 12)

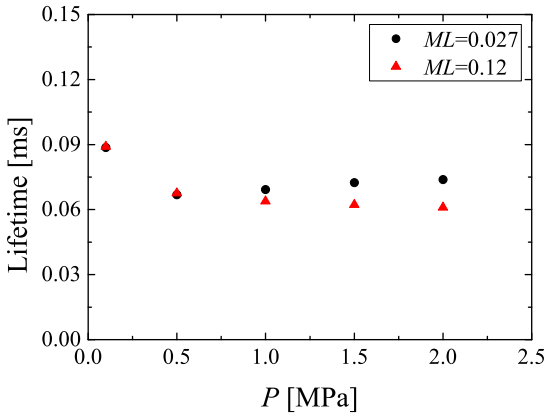

(b) T_0=1500 K (Cases 9 and 13)

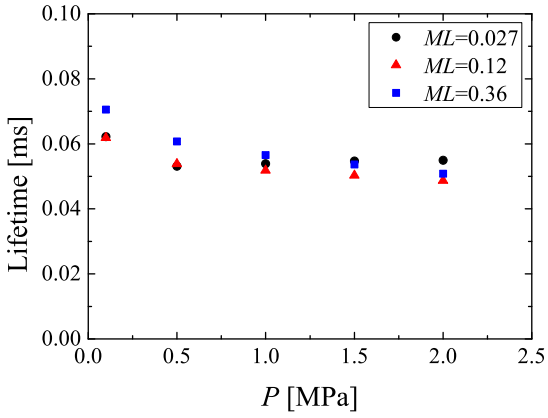

(c) T_0=2000 K (Cases 10, 14 and 15)

Figure 16: Effects of ambient pressure, P, and ML on droplet lifetime in air at initial gas temperature of (a) T_0=1000 K, (b) T_0=1500 K and (c) T_0=2000 K.

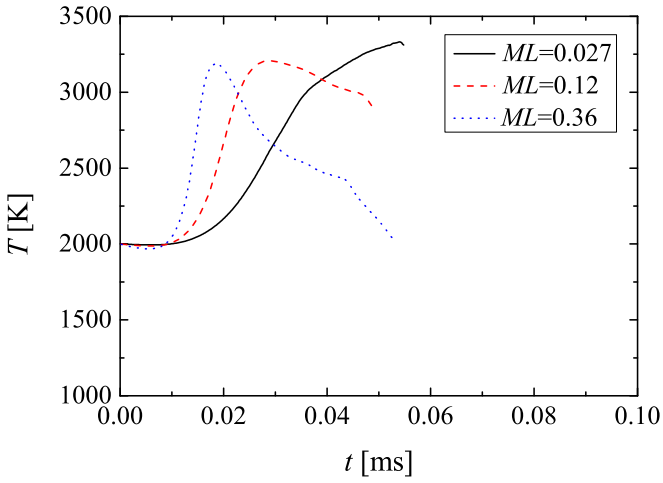

(a) T

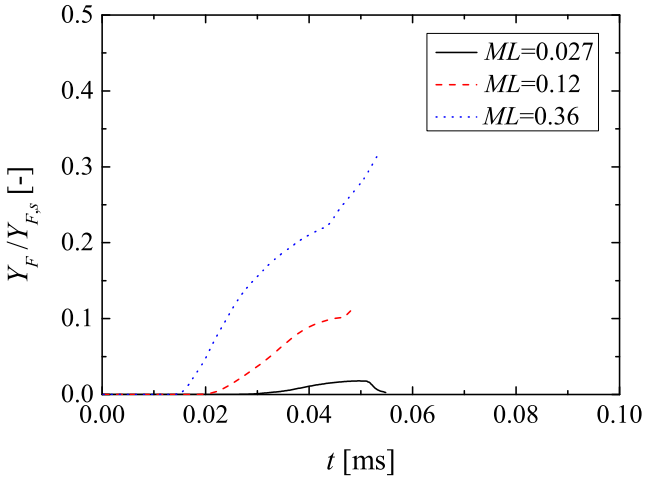

(b) $Y_F/Y_{F,s}$

Figure 17: Time variations of (a) gas temperature, T, and (b) ratio of mass fraction of evaporated fuel to vapor surface mass fraction, $Y_F/Y_{F,s}$, in air at initial gas temperature of T_0=2000 K and ambient pressure of P=2.0 MPa (see Fig.16 (c)).

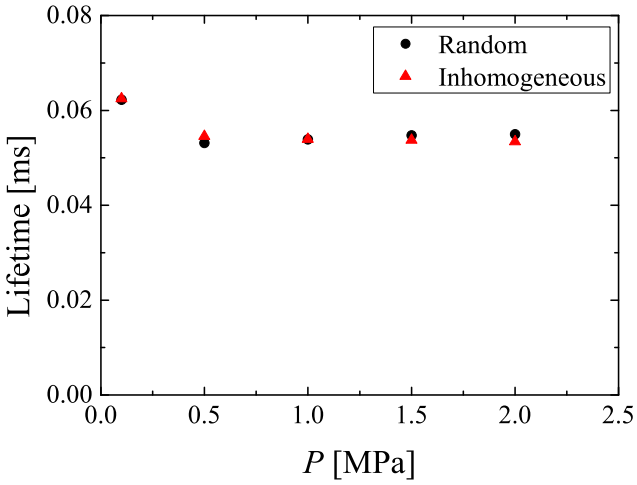

(a) ML=0.027 (without parcel model, Cases 10 and 18)

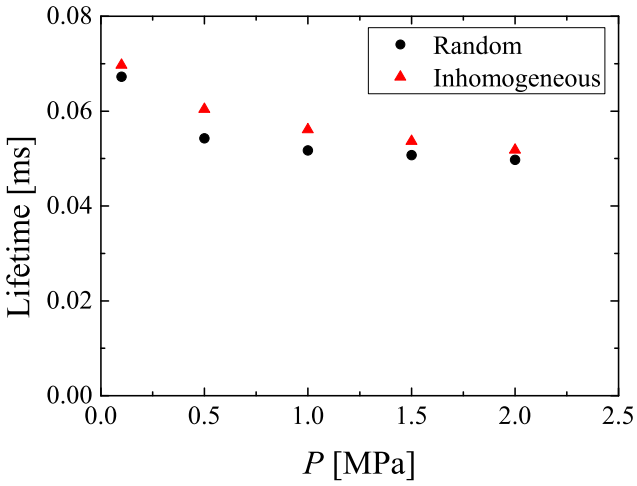

(b) ML=0.054 (with parcel model, Cases 11 and 19)

Figure 18: Effect of inhomogeneity of droplet distribution on droplet lifetime in air at initial gas temperature of T_0=2000 K for (a) ML=0.027 (without parcel model) and (b) ML=0.054 (with parcel model).